Physica B 630 (2022) 413676

Contents lists available at ScienceDirect

Physica B: Physics of Condensed Matter

journal homepage: www.elsevier.com/locate/physb

First-principles study of the influence of lone pair electrons and molecular groups on the birefringence of phosphate and fluorophosphate

Yanyan Qian [a,b], Qun Jing [a,b,*], Haiming Duan [a,b], Ming-Hsien Lee [c], Haibin Cao [d]

[a] Xinjiang Key Laboratory of Solid State Physics and Devices, Xinjiang University, 666 Shengli Road, Urumqi, 830046, China
[b] School of Physical Science and Technology, Xinjiang University, 666 Shengli Road, Urumqi, 830046, China
[c] Department of Physics, Tamkang University, New Taipei City, 25137, Taiwan
[d] Department of Physics, College of Sciences, Shihezi University, Shihezi, 832000, China

ARTICLE INFO

Keywords:
Phosphate
Fluorophosphate
Cationic and anionic groups
Birefringence
DFT investigation

ABSTRACT

As a significant nonlinear optical compound, phosphate has been wildly used in all kinds of advanced optical systems. In this work, the electronic structures, and optical properties of a series of XPO_3F and $X_3(PO_4)_2$ (X = Sn, Pb, Sr, Ba) compounds were investigated using the first-principles method in both molecular and crystal levels. The results show that introducing F atoms can lead to enhanced HOMO-LUMO gap and enlarged anisotropy of polarizability. The anionic groups give main contribution to the total birefringence of alkaline earth phosphate and fluorophosphate. As for the post-transition metal phosphate and fluorophosphate, both anionic groups and cation-centric polyhedra play a critical role in determining birefringence. The X-p (X = Sn, and Pb) states nearby the Fermi level are beneficial to get enhanced birefringence, but they do not play a vital role in determining total birefringence.

1. Introduction

Owing to their essential function in the modulation of light polarization, birefringent materials have attracted considerable academic and commercial interest in the laser industry, optical communication, polarimetry, and scientific instrumentation [1–11]. Many excellent birefringent compounds are found in borates, carbonates, phosphates, halides, and so on, such as MgF_2 [12], α-BaB_2O_4 [13], $CaCO_3$ [14], YVO_4 [15], $LiNbO_3$ [16], $Ca(BO_2)_2$ [17], whose spectral range covers ultraviolet (UV) and infrared (IR).

Recent research has suggested that introducing planar or coplanar fundamental building units (FBUs) with extreme optical anisotropy like BO_3, NO_3, CO_3, and $C_3N_3O_3$ groups [18–26] help to enhance birefringence. And introducing anionic groups parallel or parallel to the optical axis can also improve birefringence [27–29]. Additionally, introducing stereochemical active lone pairs (SCALP) electrons (such as Pb^{2+}, Bi^{3+}, Sn^{2+}, Sb^{3+}, etc.) [30–33] is a good strategy to get enhanced birefringence. For instance, α-SnF_2 [34] with SCALP electrons possesses the largest birefringence among the reported metal fluorides (0.177 @ 546 nm), which is 14 times that of MgF_2.

Phosphates have been regarded as UV and deep-ultraviolet (DUV) nonlinear optical (NLO) candidates due to their short UV absorption edges, the diversity of structures, and the easy growth of large single crystals [35,36]. While the stumbling block is their comparatively small birefringence affected by the regular tetrahedral of PO_4 whose polarization anisotropy is very small (shown in Table 1). Recently, introducing F atoms into the $(PO_4)^{3-}$ tetrahedron to form the $(PO_3F)^{2-}$ group is a new strategy to enhance optical anisotropy. The authors have calculated the dipole moment, polarizability anisotropy, and HOMO-LUMO gap of $(PO_4)^{3-}$ and $(PO_3F)^{2-}$ anionic groups using the Gaussian 09 code [37] at the B3LYP/6-31G level [38]. Herein the HOMO is the abbreviation of Highest Occupied Molecular Orbitals, and LUMO is Lowest Unoccupied Molecular Orbitals. As shown in Table 1, the obtained results show that the $(PO_3F)^{2-}$ group exhibits greater polarization anisotropy than the $(PO_4)^{3-}$ group. In addition, the larger HOMO-LUMO gap indicates that fluorophosphate has a greatly short UV cut-off edge. All calculation results demonstrate that the $(PO_3F)^{2-}$ group can enhance the birefringence and retain the benefits of the broadly ultraviolet transmittance of phosphate. Our study illustrates that introducing F atoms into fluorophosphate systems can exhibit excellent NLO performance according to the anionic group theory [39].

In this work, the molecular orbital, electronic structure, and optical properties of a series of XPO_3F and $X_3(PO_4)_2$ (X = Sn, Pb, Sr, Ba) compounds were investigated using first-principles methods. The

* Corresponding author. Xinjiang Key Laboratory of Solid State Physics and Devices, Xinjiang University, 666 Shengli Road, Urumqi, 830046, China.
E-mail address: qunjing@xju.edu.cn (Q. Jing).

https://doi.org/10.1016/j.physb.2022.413676
Received 18 August 2021; Received in revised form 30 December 2021; Accepted 8 January 2022
Available online 18 January 2022

Table 1
The obtained Dipole Moment (Px, Py, Pz), Polarizability Anisotropy of Molecular Groups (δ), HOMO−LUMO gap (E_g) of the $(PO_3F)^{2-}$ and $(PO_4)^{3-}$ Anionic Groups using Gaussian09 code.

Group	Px, Py, Pz	E_g (eV)	δ			
			266 nm	532 nm	1064 nm	2090 nm
$(PO_3F)^{2-}$	0.99, 0.28, 0.34	8.55	6.96	6.29	6.16	6.13
$(PO_4)^{3-}$	0, 0, 0	8.10	0	0	0	0

distribution of the anisotropic lone pair of electrons is determined by the electron localization functions (ELF). In addition, the author detailed analysis of the influence of crystal structures, band gap, anionic groups, and lone pair electrons on the birefringence, and try to dig out the origination of the different birefringence in fluorophosphate and phosphate. According to research, we could find that the cationic and anionic groups give the main contribution to the birefringence of phosphate and fluorophosphate, and the cationic p states also have a contribution to the birefringence. Those perceptions will guide and accelerate the exploration of excellent birefringent and NLO materials in fluorophosphate compounds.

2. Calculation details

To better expound the electronic structures and optical properties of XPO_3F and $X_3(PO_4)_2$ (X = Sn, Pb, Sr, Ba), the first-principles calculations were performed using the plane-wave pseudopotential code CASTEP [40,41] based on the density functional theory (DFT) [42,43]. The Crystallographic Information File (CIF) of XPO_3F and $X_3(PO_4)_2$ (X = Sn, Pb, Sr, Ba) compounds are obtained from the inorganic crystal structure database (ICSD, Version 4.5.0). During the calculation, the generalized gradient approximation(GGA) [44] with Perdew-Burke-Ernzerhof (PBE) [45] functional and the norm-conserving pseudopotential [46,47] were adopted. The following orbital electrons were treated as valence electrons Sn:$5s^25p^2$, Pb:$5s^25p^65d^{10}6s^26p^2$, Sr:$4s^24p^65s^2$, Ba:$5s^25p^66s^2$, P:$3s^23p^3$, O:$2s^22p^4$, F:$2s^22p^5$. The kinetic energy cut-offs were set as 940 eV for XPO_3F and 830 eV for $X_3(PO_4)_2$ (X = Sn, Pb, Sr, Ba). The Monkhorst-Pack k-points of those compounds were set as 5 × 2 × 4 ($SnPO_3F$), 5 × 4 × 4($PbPO_3F$), 5 × 4 × 4($SrPO_3F$), 3 × 3 × 3($BaPO_3F$), 2 × 5 × 2($Sn_3(PO_4)_2$), 5 × 5 × 5($Pb_3(PO_4)_2$), 6 × 6 × 6($Sr_3(PO_4)_2$) and 5 × 5 × 5($Ba_3(PO_4)_2$) with a density of 0.04/Å in the first Brillouin zone(BZ). Other calculation parameters and convergence criteria adopted default value of the CASTEP code. After the electronic structures were obtained, the OptaDOS [48,49] code is used to get the real and imaginary parts of the dielectric constant, and then the refractive index n along optical principle axes and the birefringence Δn defined as the difference of refractive indices along optical principle axes were obtained. During the calculation, a scissors operator was introduced to shift up the conduction band and get more reliable birefringence. The scissors value is defined as the difference between the HSE06 bandgap and GGA/PBE bandgap. The HSE06 [50–52] hybrid functional implemented in PWMAT [53,54] code

Table 2
The Distortion Index of XPO_3F and $X_3(PO_4)_2$ (Sn, Pb, Sr, Ba) compounds.

Crystal	Group	Distortion index	Crystal	Group	Distortion index
$SnPO_3F$	PO_3F	0.0334	$Sn_3(PO4)_2$	PO_4	0.0072
	SnO_3	0.0137		SnO_3	0.0247
$PbPO_3F$	PO_3F	0.0334	$Pb_3(PO4)_2$	PO_4	0.0189
	PbO_7F_2	0.0443		PbO_{10}	0.0316
$SrPO_3F$	PO_3F	0.0103	$Sr_3(PO4)_2$	PO_4	0.0069
	SrO_7F_2	0.0442		SrO_{10}	0.0000
$BaPO_3F$	PO_3F	0.0103	$Ba_3(PO4)_2$	PO_4	0.0017
	BaO_7F_2	0.0358		BaO_{10}	0.0150

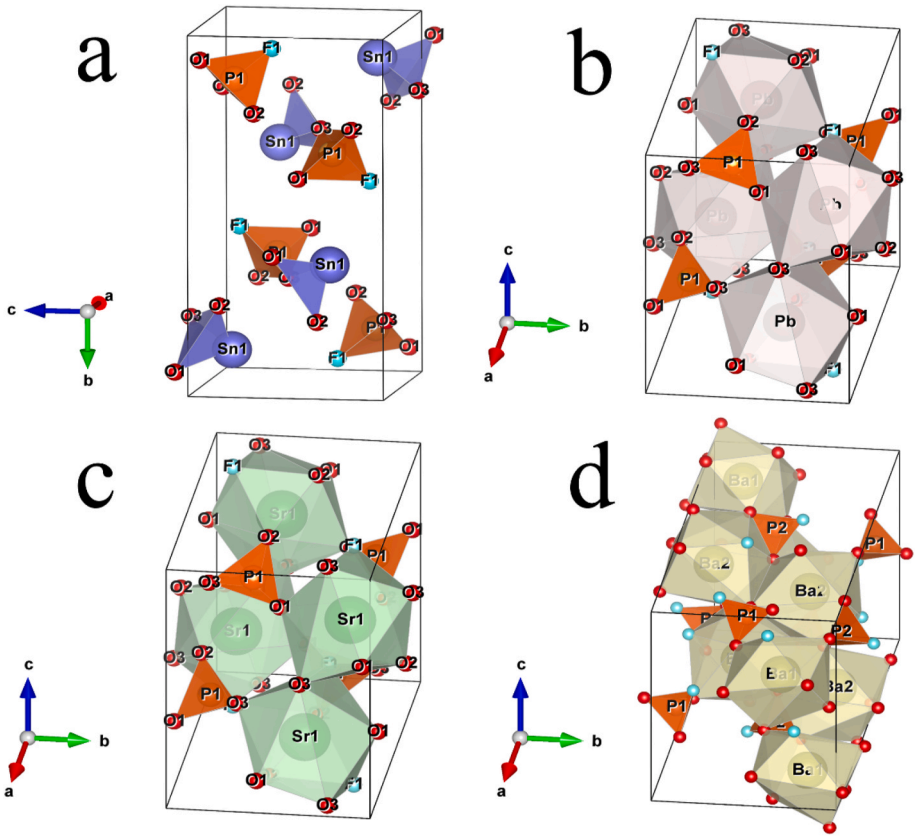

Fig. 1. Crystal structures of (a) $SnPO_3F$, (b) $PbPO_3F$, (c)$SrPO_3F$ and (d)$BaPO_3F$.

Table 3
Space Groups, Calculated Band Gaps with GGA/PBE functional and HSE06 hybrid functional and The Birefringence (Δn) at 1064 nm concerning scissors operator.

Crystal	Space group	E_g(PBE) (eV)	E_g(HSE06) (eV)	Birefringence
$SnPO_3F$	$P2_1/c$	3.46	4.83	0.075
$PbPO_3F$*	$P2_1/c$	4.58	5.36	0.061
$SrPO_3F$	$P2_1/c$	5.74	7.18	0.034
$BaPO_3F$	$P2_1/c$	5.47	7.09	0.007
$Sn_3(PO_4)_2$	$P2_1/c$	2.86	4.28	0.040
$Pb_3(PO_4)_2$	R $\bar{3}$ 2/m	3.36	4.15	0.011
$Sr_3(PO_4)_2$	R $\bar{3}$ 2/m	5.97	7.38	0.004
$Ba_3(PO_4)_2$	R $\bar{3}$ 2/m	5.39	6.96	0.004

$PbPO_3F$*: $PbPO_3F$ was obtained by replacing the Ba atom in $BaPO_3F$ with a Pb atom.

is used to get bandgap comparable with experimental values, and it was also used to get the projected band structure to see the states nearby the Fermi level, and the scissors values.

3. Result and discussion

Before deeply comprehending the electronic structures and optical properties, the authors would review their geometries firstly. The crystal structures of XPO_3F and $X_3(PO_4)_2$ (X = Sn, Pb, Sr, Ba) are shown in Fig. 1, Fig. S1, and Table 2. The XPO_3F and $X_3(PO_4)_2$ (X = Sn, Pb, Sr, Ba) crystallize in the $P2_1/c$ and R $\bar{3}$ 2/m centrosymmetric structures. After detailed check out the geometries, one can ascertain that these compounds own isolated distorted tetrahedrons of $(PO_3F)^{2-}$ groups and $(PO_4)^{3-}$ groups, respectively. And these compounds also own different cation-centric polyhedra (such as SnO_3, PbO_{10} et al.) due to different cationic coordination environments, and these cationic groups are all connected to the $(PO_3F)^{2-}$ tetrahedron by sharing oxygen atoms.

The distortion indices of different polyhedra are also calculated using Baur's method [55] implemented in VESTA code [56]. As shown in Table 2, the $(PO_3F)^{2-}$ group has a greater distortion degree than the $(PO_4)^{3-}$ group. Take $SnPO_3F$ and $Sn_3(PO_4)_2$ for example, the distortion indices of PO_3F (0.0334) in $SnPO_3F$ are larger than PO_4 (0.0072) in $Sn_3(PO_4)_2$. In addition, introducing F atoms into the cationic polyhedron can also enhance the distortion indices. For example, the distortion index of BaO_7F_2 (0.0358) in $BaPO_3F$ is larger than BaO_{10} (0.0150) in $Ba_3(PO_4)_2$. Noting that although the distortion index of SnO_3 in $SnPO_3F$ is smaller than other cationic groups in fluorophosphates, $SnPO_3F$ still owns the largest birefringence (as shown in Table 3), hence the authors believe that the electronic structures rather than geometries play an important role in determining the optical properties.

3.1. The contribution of electronic structures to birefringence

Using the method described above, the electronic structures and refractive indices are obtained. The obtained GGA/PBE band structures along the high-symmetry points of the first Brillouin zone are shown in Fig. 2 and Fig. S2. $SnPO_3F$ is a direct bandgap semiconductor with 3.46 eV, the other compounds are all indirect bandgap semiconductors with bandgap of 5.74 eV ($SrPO_3F$), 5.47 eV ($BaPO_3F$), 4.58 eV ($PbPO_3F$), 5.97 eV ($Sr_3(PO_4)_2$), 5.36 eV ($Ba_3(PO_4)_2$), 3.36 eV ($Pb_3(PO_4)_2$) and 2.86 eV ($Sn_3(PO_4)_2$) respectively. It is widely known that the calculated bandgap by the GGA can cause a quantitative underestimation of the bandgap due to the discontinuity of exchange-correlation energy [57,58], thus the Heyd-Scuseria-Ernzerhof (HSE06) hybrid functional implemented in the PWMAT which can obtain values comparable with experimental values was employed to characterize the bandgap of those compounds. As shown in Table 3, the HSE06 functional yielded bandgaps of 4.83eV ($SnPO_3F$), 5.36eV ($PbPO_3F$), 7.18eV ($SrPO_3F$), 7.09eV ($BaPO_3F$), 4.28eV ($Sn_3(PO_4)_2$), 4.15eV ($Pb_3(PO_4)_2$), 7.38eV ($Sr_3(PO_4)_2$), 6.96eV ($Ba_3(PO_4)_2$), respectively.

The acquired refractive indices and birefringence are shown in Fig. 3, Fig. S3, and Table 3. The one containing post-transition metal atoms own relatively large birefringence, that's $SnPO_3F$ (0.075)> $PbPO_3F$ (0.061)> $SrPO_3F$ (0.034)> $BaPO_3F$ (0.007), and $Sn_3(PO_4)_2$ (0.040)> $Pb_3(PO_4)_2$ (0.011)> $Ba_3(PO_4)_2$ (0.004))> $Sr_3(PO_4)_2$ (0.004). Moreover, compared to phosphate, fluorophosphate owns larger birefringence. For example, the birefringence of $SnPO_3F$ (0.075) is larger than $Sn_3(PO4)_2$, and $PbPO_3F$ (0.061) is larger than $Pb_3(PO_4)_2$. Therefore, we believe that the $(PO_3F)^{2-}$ anionic groups can significantly increase the birefringence of the fluorophosphate and will be further demonstrated below.

3.2. The contribution of anionic groups to birefringence

Let's turn our attention to the role played by anionic groups to

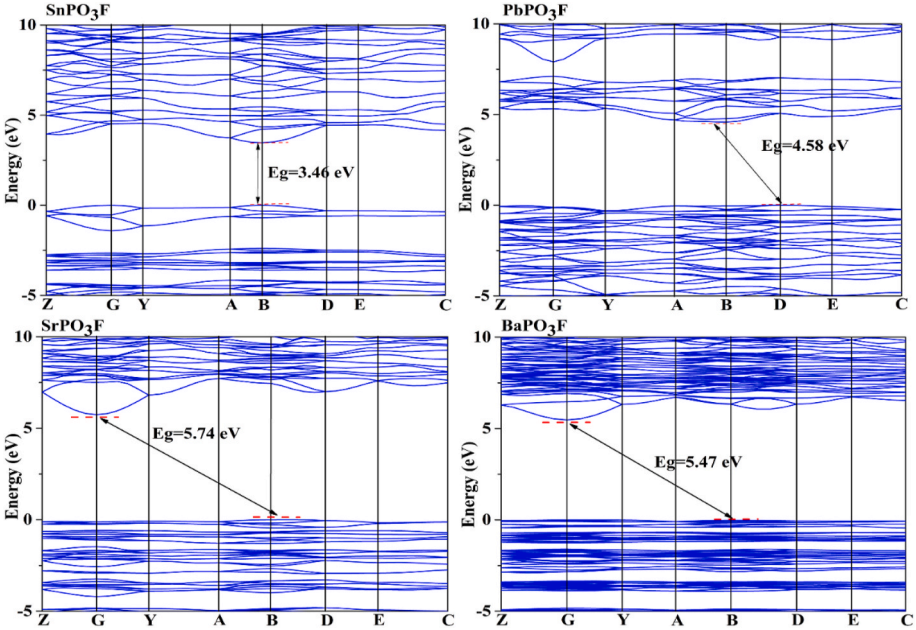

Fig. 2. Band structures of XPO_3F (X = Sn, Pb, Sr, Ba) determined using GGA/PBE functional implemented in CASTEP code.

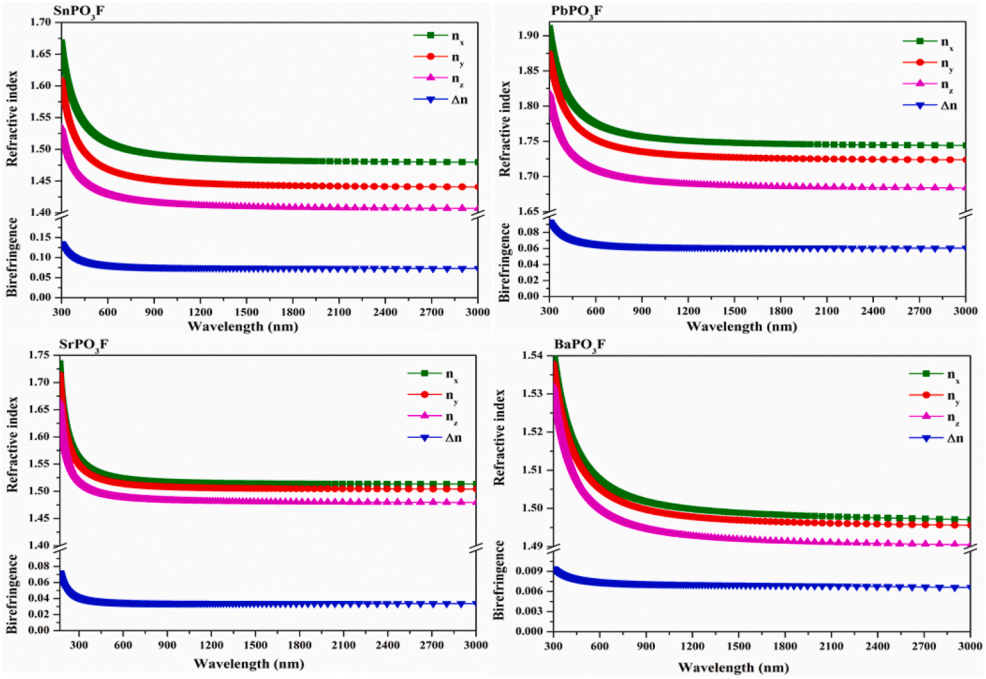

Fig. 3. The refractive indices and birefringence values of XPO_3F (X = Sn, Pb, Sr, Ba) were calculated by the OptaDOS code.

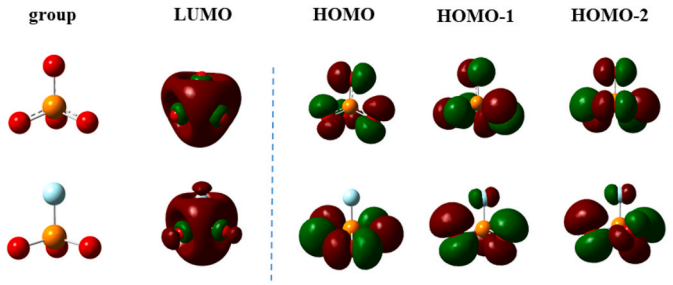

Fig. 4. Frontier molecular orbitals of the $(PO_4)^{3-}$ and $(PO_3F)^{2-}$ anionic groups. The red, yellow, and cyan balls represent the oxygen, phosphorus, and fluorine atoms, respectively. (For interpretation of the references to colour in this figure legend, the reader is referred to the Web version of this article.)

birefringence. The anionic groups' contribution was first investigated at the B3LYP/6-31G level using the Gaussian09 code (shown in Table 1). Fig. 4 shows the frontier molecular orbital diagrams of $(PO_4)^{3-}$ and $(PO_3F)^{2-}$ anionic groups. As shown in Fig. 4, the $(PO_3F)^{2-}$ anionic groups own significant anisotropic electronic distribution in HOMO, HOMO-1, and HOMO-2. Herein the HOMO-1 is the adjacent molecular state lower than HOMO, and HOMO-2 is the adjacent molecular state lower than HOMO-1. For $(PO_3F)^{2-}$ anionic groups (shown in the bottom of Fig. 4), the electronic distribution mainly localized at the bottom of HOMO (mainly around oxygen atoms), and almost no electrons can be found in the upper of HOMO, very little electrons can be found around the F atoms in HOMO-1, and HOMO-2. While as for the $(PO_4)^{3-}$ anionic groups, the electronic distribution can be found around all oxygen atoms, which make the $(PO_4)^{3-}$ anionic groups own isotropic electronic distribution. The anisotropic electronic distribution of $(PO_3F)^{2-}$ anionic groups are beneficial to acquire relatively large polarization anisotropy leading to large birefringence.

To further investigate the contribution of different ions to total birefringence, a real-space atom-cutting (RSAC) [58] method was used in XPO_3F and $X_3(PO_4)_2$ (X = Sn, Pb, Sr, Ba). According to the rule of keeping the cutting spheres in contact and without overlap, the cutting radii of Sn, Pb, Sr, Ba, P, O, and F were set as 1.55, 1.50, 1.13, 1.37, 0.95, 1.10, and 0.86 Å, respectively. The obtained RSAC results are shown in Table 4. Noting that, as shown in Fig. S3, the birefringence of $X_3(PO_4)_2$ (X = Sr, Ba) is very small (only 0.004, and 0.004, respectively). With consideration of numerical calculation error, the authors have not performed the RSAC operation on these two compounds. Based on the RSAC method, the birefringence of different ions and anionic groups are obtained and several observations can be obtained as follows: (1) For those alkaline earth fluorophosphate, the anionic groups give the main contribution to the total birefringence, and the alkaline earth atoms' contribution is so little that it even can be ignored. For example, the birefringence of the $(PO_3F)^{2-}$ group (0.032) is almost equivalent to the $SrPO_3F$ crystal (0.034). (2) For the post-transition metal phosphate and fluorophosphate, i.e. XPO_3F and $X_3(PO_4)_2$ (X = Sn, Pb), both anionic groups and cation-centric polyhedra play an important role in determining the birefringence. Take $PbPO_3F$ compound for example, the birefringence of the PbO_7F_2 polyhedron (0.036) is comparable to the PO_3F anionic group (0.042). (3) It is worth noting that the cationic

Table 4
The obtained refractive indices and birefringence of different polyhedra in title compounds.

Crystal		n_x	n_y	n_z	Δn
$SnPO_3F$	Total	1.488	1.448	1.412	0.076
	SnO_3	1.272	1.247	1.201	0.071
	PO_3F	1.215	1.202	1.187	0.028
$PbPO_3F$	Total	1.752	1.731	1.690	0.062
	PbO_7F_2	1.634	1.618	1.598	0.036
	PO_3F	1.481	1.470	1.439	0.042
$SrPO_3F$	Total	1.516	1.506	1.481	0.034
	Sr	1.139	1.137	1.133	0.007
	PO_3F	1.413	1.400	1.381	0.032
$BaPO_3F$	Total	1.500	1.498	1.493	0.007
	Ba	1.262	1.262	1.258	0.004
	PO_3F	1.487	1.471	1.470	0.017
$Sn_3(PO_4)_2$	Total	1.558	1.533	1.518	0.040
	SnO_3	1.529	1.496	1.488	0.041
	PO_4	1.226	1.212	1.211	0.015
$Pb_3(PO_4)_2$	Total	1.936	1.936	1.925	0.011
	PbO_{10}	1.948	1.948	1.935	0.013
	PO_4	1.685	1.685	1.682	0.003

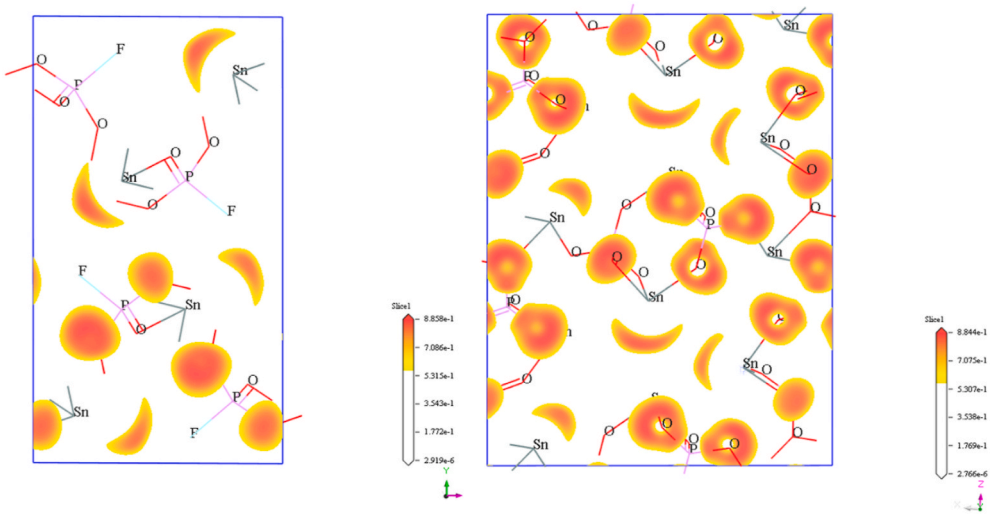

Fig. 5. The electron localization functions (ELFs) of $SnPO_3F$ and $Sn_3(PO_4)_2$.

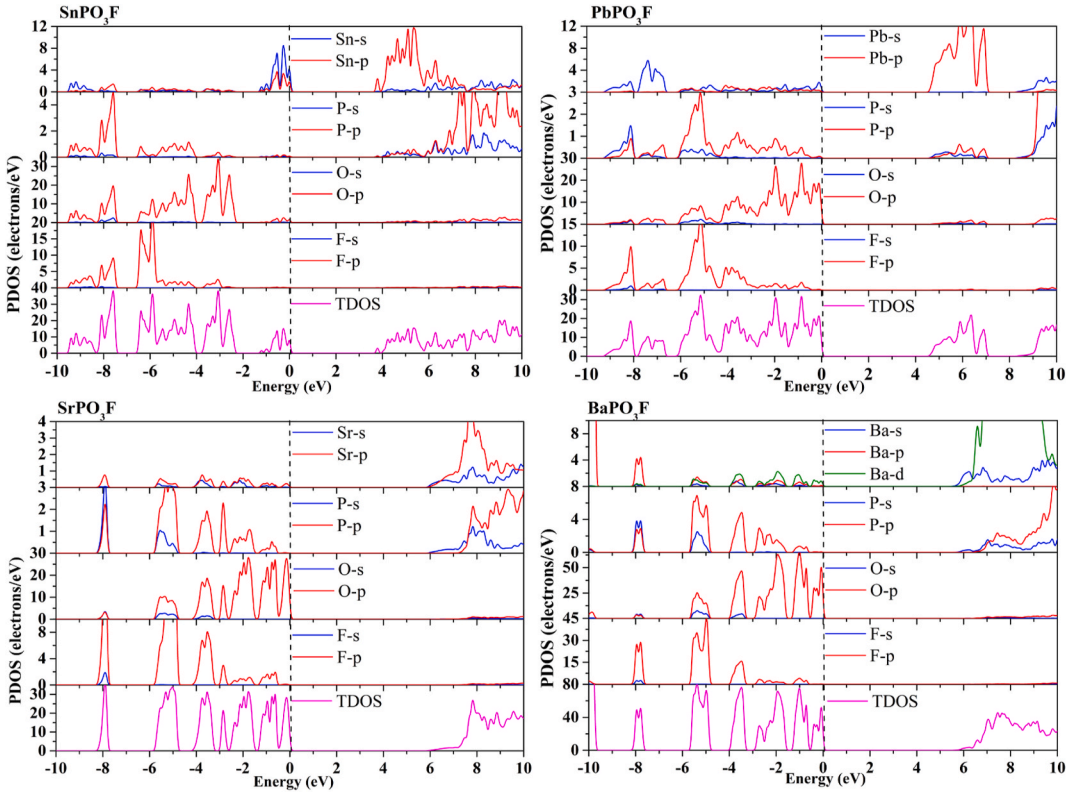

Fig. 6. The projected densities of states (PDOSs) of XPO_3F (X = Sn, Pb, Sr, Ba).

groups give more contribution to the total birefringence in other post-transition metal phosphate and fluorophosphate. For example, the birefringence of SnO_3 in $SnPO_3F$ (0.071) is larger than PO_3F (0.028), and the birefringence of SnO_3 in $Sn_3(PO_4)_2$ (0.041) is larger than PO_4 (0.015).

3.3. The lone pair electronic distribution and their contribution

The stereochemistry active lone-pair electronic distribution is further confirmed by the electron localization functions (ELF). To better display the electronic characteristics of the lone pair, the ELF of the $SnPO_3F$ and $Sn_3(PO_4)_2$ compound with the more obvious lone pair electronic effect was produced (shown in Fig. 5). Here, crescent-shaped ELFs were observed around the Sn atoms, indicative of asymmetric lone-pair electron distributions around these atoms. Such asymmetric lone pair electrons distributions could lead to enhanced birefringence and more details will be shown below.

Meanwhile, the total density of states (TDOS) and projected densities of states (PDOS) of XPO_3F and $X_3(PO_4)_2$ (X = Sn, Pb, Sr, Ba) are exhibited in Fig. 6 and Fig. S6. Clearly, the cation-sp, O-p, F-p, and P-sp states were found at the top of the valence band (VB) and the bottom of the conduction band (CB). Noting that not only the hybrid P–O states, but also the hybrid Sn–O and hybrid Pb–O states are found near the Fermi level. The hybrid P–O states, Sn–O states, and Pb–O states can also

Table 5
The PDOS integration of XPO_3F and $X_3(PO4)_2$ (X = Sn, Pb, Sr, Ba) in [-6, 0] eV.

Crystal	Band-gap	birefringence	PDOS integration			
			$S_{(X\text{-}s)}$	$S_{(X\text{-}p)}$	$S_{(O\text{-}p)}$	R
$SnPO_3F$	3.46	0.075	4.97	2.97	44.21	5.69%
$PbPO_3F$	4.58	0.061	3.29	2.75	56.33	4.40%
$Sn_3(PO_4)_2$	2.86	0.034	14.88	9.10	109.00	6.84%
$Pb_3(PO_4)_2$	3.36	0.011	2.06	2.23	36.72	5.43%

be verified by the projected band structures diagram shown in Fig. S7. According to the revised model suggested by Walsh [59], the hybrid Sn sp- O p (Pb sp-O p) states below the Fermi level should own a similar character like stereochemistry activate lone pair electronic distribution.

After detailed checkout the PDOS shown in Fig. 6, the authors believe the cationic p states nearby the Fermi level would play some role in determining the birefringence. To further illustrate the contribution from cationic p states to the total birefringence, the PDOS of those compounds were integrated from [−6, 0] eV and then the ratio of cation-p state to hybrid cation-oxygen states are calculated using the formula like R(cation-p) = X(cation-p)/((X(cation-p) + X(cation-s) +X(O-p)), and where the X(cation-s), X(cation-p), X(O-p), are the intensities of cation-s states, cation-p states, O-p states, respectively. Electron transitions coming from deep energy give minor contribution to the optical properties, so states lower than −6 eV were omitted. As shown in Table 5, the sequence of R(X-p) is $PbPO_3F$ (0.044) <$SnPO_3F$ (0.056), $Pb_3(PO_4)_2$(0.054) <$Sn_3(PO_4)_2$(0.068), which is consistent with the trend found in birefringence, implying that the Sn-p and Pb-p states indeed help to enhance the birefringence. The authors must point out that the ratio of cationic p states is smaller than oxygen atoms, indicating they give limited contribution to total birefringence. In a word, the X-p (X = Sn, and Pb) states nearby the Fermi level are beneficial to get enhanced birefringence, but they do not play a vital role in determining total birefringence.

4. Conclusion

In summary, this work systematically investigated the crystal structure, electronic structures, and optical properties of XPO_3F, and $X_3(PO_4)_2$ (X = Sn, Pb, Sr, Ba) using the first-principles method in molecular and crystal levels. The results show that: (1) For the alkaline earth phosphate and fluorophosphate, the anionic groups give the main contribution to the total birefringence, the alkaline earth atoms' contribution can be ignored. (2) For the post-transition metal phosphate and fluorophosphate, both anionic groups and cation-centered polyhedra play an important role in determining birefringence. (3) The obtained birefringence values of XPO_3F and $X_3(PO_4)_2$(X = Sn, Pb, Sr, Ba) followed the sequence Sn > Pb > Sr > Ba. The X-p (X = Sn, and Pb) states nearby the Fermi level are beneficial to get enhanced birefringence, but they do not play a vital role in determining total birefringence. The obtained results can be used to design novel UV/DUV NLO compounds.

Credit author statement

Yanyan Qian: Formal analysis, Data curation, Writing – original draft. Qun Jing: Supervision, Project administration, Writing – review & editing. Haiming Duan: Software. Ming-Hsien Lee: Method & Software. Haibin Cao: Software.

Declaration of competing interest

The authors declare that they have no known competing financial interests or personal relationships that could have appeared to influence the work reported in this paper.

Acknowledgment

This work is supported by the National Natural Science Foundation of China (Grant No. 11864040), the Natural Science Foundation of Xinjiang Uygur Autonomous Region of China (Grant No. 2018D01C072), and Tianshan Innovation Team Program of Xinjiang Uygur Autonomous Region (Grant No. 2020D14038).

Appendix A. Supplementary data

Supplementary data to this article can be found online at https://doi.org/10.1016/j.physb.2022.413676.

References

[1] F. Flossmann, U.T. Schwarz, M. Maier, M.R. Dennis, Polarization singularities from unfolding an optical vortex through a birefringent crystal, Phys. Rev. Lett. 95 (25) (2005) 253901.
[2] M. Li, H. Pan, Y. Tong, C. Chen, H. Zeng, All-optical ultrafast polarization switching of terahertz radiation by impulsive molecular alignment, Opt Lett. 36 (18) (2011) 3633–3635.
[3] P. Hlubina, D. Ciprian, L. Knyblová, Interference of white light in the tandem configuration of birefringent crystal and sensing birefringent fiber, Opt Commun. 260 (2) (2006) 535–541.
[4] G. Shi, Y. Wang, F. Zhang, B. Zhang, Z. Yang, X. Hou, S. Pan, K.R. Poeppelmeier, Finding the next deep-ultraviolet nonlinear optical material: $NH_4B_4O_6F$, J. Am. Chem. Soc. 139 (31) (2017) 10645–10648.
[5] H. Wu, S. Pan, K.R. Poeppelmeier, H. Li, D. Jia, Z. Chen, X. Fan, Y. Yang, J. M. Rondinelli, H. Luo, $K_3B_6O_{10}Cl$: a new structure analogous to perovskite with a large second harmonic generation response and deep UV absorption edge, J. Am. Chem. Soc. 133 (20) (2011) 7786–7790.
[6] Z. Yang, A. Tudi, B.-H. Lei, S. Pan, Enhanced nonlinear optical functionality in birefringence and refractive index dispersion of the deep-ultraviolet fluorooxoborates, Science China Materials 63 (8) (2020) 1480–1488.
[7] Z. Yang, B.-H. Lei, W. Zhang, S. Pan, Module-analysis-assisted design of deep ultraviolet fluorooxoborates with extremely large gap and high structural stability, Chem. Mater. 31 (8) (2019) 2807–2813.
[8] B.-H. Lei, S. Pan, Z. Yang, C. Cao, D.J. Singh, Second harmonic generation susceptibilities from symmetry adapted Wannier functions, Phys. Rev. Lett. 125 (18) (2020) 187402.
[9] B.-H. Lei, Z. Yang, H. Yu, C. Cao, Z. Li, C. Hu, K.R. Poeppelmeier, S. Pan, Module-guided design scheme for deep-ultraviolet nonlinear optical materials, J. Am. Chem. Soc. 140 (34) (2018) 10726–10733.
[10] W. Jin, W. Zhang, A. Tudi, L. Wang, X. Zhou, Z. Yang, S. Pan, Fluorine-driven enhancement of birefringence in the fluorooxosulfate: a deep evaluation from a joint experimental and computational study, Adv. Sci. (2021) 2003594.
[11] T. Tong, W. Zhang, Z. Yang, S. Pan, Series of crystals with giant optical anisotropy: a targeted strategic research, Angew. Chem. Int. Ed. 60 (3) (2021) 1332–1338.
[12] M.J. Dodge, Refractive properties of magnesium fluoride, Appl. Opt. 23 (12) (1984) 1980–1985.
[13] S. Wu, G. Wang, J. Xie, X. Wu, Y. Zhang, X. Lin, Growth of large birefringent α-BBO crystal, J. Cryst. Growth 245 (1–2) (2002) 84–86.
[14] G. Ghosh, Dispersion-equation coefficients for the refractive index and birefringence of calcite and quartz crystals, Opt Commun. 163 (1–3) (1999) 95–102.
[15] H.T. Luo, T. Tkaczyk, E.L. Dereniak, K. Oka, R. Sampson, High birefringence of the yttrium vanadate crystal in the middle wavelength infrared, Opt Lett. 31 (5) (2006) 616–618.
[16] J.R. Devore, Refractive indices of rutile and sphalerite, J. Opt. Soc. Am. 41 (6) (1951), 266-266.
[17] X. Chen, B. Zhang, F. Zhang, Y. Wang, M. Zhang, Z. Yang, K.R. Poeppelmeier, S. Pan, Designing an excellent deep-ultraviolet birefringent material for light polarization, J. Am. Chem. Soc. 140 (47) (2018) 16311–16319.
[18] Z. Li, F. Liang, Y. Guo, Z. Lin, J. Yao, G. Zhang, W. Yin, Y. Wu, C. Chen, $Ba_2M(C_3N_3O_3)_2$ (M = Mg, Ca): potential UV birefringent materials with strengthened optical anisotropy originating from the $(C_3N_3O_3)^{3-}$ group, J. Mater. Chem. C 6 (47) (2018) 12879–12887.
[19] J. Lu, Y.-K. Lian, L. Xiong, Q.-R. Wu, M. Zhao, K.-X. Shi, L. Chen, L.-M. Wu, How to maximize birefringence and nonlinearity of π-conjugated cyanurates, J. Am. Chem. Soc. 141 (40) (2019) 16151–16159.
[20] B. Wu, D. Tang, N. Ye, C. Chen, Linear and nonlinear optical properties of the $KBe_2BO_3F_2$ (KBBF) crystal, Opt. Mater. 5 (1) (1996) 105–109.
[21] G. Zou, N. Ye, L. Huang, X. Lin, Alkaline-alkaline earth fluoride carbonate crystals $ABCO_3F$ (A = K, Rb, Cs; B = Ca, Sr, Ba) as nonlinear optical materials, J. Am. Chem. Soc. 133 (49) (2011) 20001–20007.
[22] X. Dong, L. Huang, Q. Liu, H. Zeng, Z. Lin, D. Xu, G. Zou, Perfect balance harmony in $Ba_2NO_3(OH)_3$: a beryllium-free nitrate as a UV nonlinear optical material, Chem. Commun. 54 (45) (2018) 5792–5795.
[23] X. Wang, Y. Wang, B. Zhang, F. Zhang, Z. Yang, S. Pan, CsB_4O_6F: a congruent-melting deep-ultraviolet nonlinear optical material by combining superior functional units, Angew. Chem. Int. Ed. 56 (45) (2017) 14119–14123.

[24] Q. Jing, G. Yang, Z. Chen, X. Dong, Y. Shi, A joint strategy to evaluate the microscopic origin of the second-harmonic-generation response in nonpolar $ABCO_3F$ compounds, Inorg. Chem. 57 (3) (2018) 1251–1258.
[25] Z. Zhang, Y. Wang, B. Zhang, Z. Yang, S. Pan, Polar fluorooxoborate NaB_4O_6F: a promising material for ionic conduction and nonlinear optics, Angew. Chem. 57 (22) (2018) 6577–6581.
[26] B. Zhang, E. Tikhonov, C. Xie, Z. Yang, S. Pan, Prediction of fluorooxoborates with colossal second harmonic generation (SHG) coefficients and extremely wide band gaps: towards modulating properties by tuning the BO_3/BO_3F ratio in layers, Angew. Chem. 131 (34) (2019) 11852–11856.
[27] Y. Wang, B. Zhang, Z. Yang, S. Pan, Cation-tuned synthesis of fluorooxoborates: towards optimal deep-ultraviolet nonlinear optical materials, Angew. Chem. Int. Ed. 57 (8) (2018) 2150–2154.
[28] H. Wu, H. Yu, Z. Yang, X. Hou, X. Su, S. Pan, K.R. Poeppelmeier, J.M. Rondinelli, Designing a deep-ultraviolet nonlinear optical material with a large second harmonic generation response, J. Am. Chem. Soc. 135 (11) (2013) 4215–4218.
[29] M. Mutailipu, Z. Min, B. Zhang, L. Wang, Z. Yang, Z. Xin, S. Pan, $SrB_5O_7F_3$ functionalized with $[B_5O_9F_3]^{6-}$ chromophores: accelerating the rational design of deep: ltraviolet nonlinear optical materials, Angew. Chem. 130 (21) (2018) 6203–6207.
[30] F. Liang, L. Kang, Z. Lin, Y. Wu, Mid-infrared nonlinear optical materials based on metal chalcogenides: structure–property relationship, Cryst. Growth Des. 17 (4) (2017) 2254–2289.
[31] C. Hu, B. Zhang, B.-H. Lei, S. Pan, Z. Yang, Advantageous units in antimony sulfides: exploration and design of infrared nonlinear optical materials, ACS Appl. Mater. Interfaces 10 (31) (2018) 26413–26421.
[32] M.-L. Liang, C.-L. Hu, F. Kong, J.-G. Mao, $BiFSeO_3$: an excellent SHG material designed by aliovalent substitution, J. Am. Chem. Soc. 138 (30) (2016) 9433–9436.
[33] X. Shi, Q. Jing, Z. Chen, M.H. Lee, H. Ding, Different mechanism of response of asymmetric lone pair electrons around ns^2 cations to birefringence and second harmonic generation, J. Appl. Phys. 128 (11) (2020) 113104.
[34] J. Guo, A. Tudi, S. Han, Z. Yang, S. Pan, alpha-SnF_2 : a UV birefringent material with large birefringence and easy crystal growth, Angew. Chem. Int. Ed. 60 (7) (2021) 3540–3544.
[35] B. Zhang, G. Shi, Z. Yang, F. Zhang, S. Pan, Fluorooxoborates: beryllium-free deep-ultraviolet nonlinear optical materials without layered growth, Angew. Chem. Int. Ed. 56 (14) (2017) 3916–3919.
[36] G. Han, Y. Wang, B. Zhang, S. Pan, Fluorooxoborates: ushering in a new era of deep ultraviolet nonlinear optical materials, Chemistry 24 (67) (2018) 17638–17650.
[37] M.J. Frisch, G.W. Trucks, H.B. Schlegel, G.E. Scuseria, M.A. Robb, A.R. Cheeseman, G. Scalmani, V. Barone, B. Mennucci, G.A. Petersson, H. Nakatsuji, M. Caricato, X. Li, H.P. Hratchian, A.F. Izmaylov, J. Bloino, G. Zheng, J.L. Sonnenberg, M. Hada, M. Ehara, K. Toyota, R. Fukuda, J. Hasegawa, M. Ishida, T. Nakajima, Y. Honda, O. Kitao, H. Nakai, T. Vreven, J.A. Montgomery, J.E. Peralta Jr., F. Ogliaro, M. Bearpark, J.J. Heyd, E. Brothers, K.N. Kudin, V.N. Staroverov, T. Keith, R. Kobayashi, J. Normand, K. Raghavachari, A. Rendell, J.C. Burant, S.S. Iyengar, J. Tomasi, M. Cossi, N. Rega, J.M. Millam, M. Klene, J.E. Knox, J.B. Cross, V. Bakken, C. Adamo, J. Jaramillo, R. Gomperts, R.E. Stratmann, O. Yazyev, A. J. Austin, R. Cammi, C. Pomelli, J.W. Ochterski, R.L. Martin, K. Morokuma, V. G. Zakrzewski, G.A. Voth, P. Salvador, J.J. Dannenberg, S. Dapprich, A.D. Daniels, O. Farkas, J.B. Foresman, J.V. Ortiz, J. Cioslowski, D.X. Fox, Gaussian 09, Revision E.01, Gaussian, Inc., Wallingford CT, 2013.
[38] S.H. Vosko, L. Wilk, M. Nusair, Accurate spin-dependent electron liquid correlation energies for local spin density calculations: a critical analysis, Can. J. Phys. 58 (8) (1980) 1200–1211.
[39] C. Chen, Y. Wu, R. Li, The anionic group theory of the non-linear optical effect and its applications in the development of new high-quality NLO crystals in the borate series, Int. Rev. Phys. Chem. 8 (1) (1989) 65–91.
[40] S.J. Clark, M.D. Segall, C.J. Pickard, P.J. Hasnip, M.I.J. Probert, K. Refson, M. C. Payne, First-principles methods using CASTEP, Z. für Kristallogr. - Cryst. Mater. 220 (5–6) (2005) 567–570.
[41] V. Milman, K. Refson, S. Clark, C. Pickard, J. Yates, S.P. Gao, P. Hasnip, M. Probert, A. Perlov, M. Segall, Electron and vibrational spectroscopies using DFT, plane waves and pseudopotentials: CASTEP implementation, J. Mol. Struct.: THEOCHEM 954 (1–3) (2010) 22–35.
[42] D. Vanderbilt, Soft self-consistent pseudopotentials in a generalized eigenvalue formalism, Phys. Rev. B 41 (11) (1990) 7892–7895.
[43] W. Kohn, Nobel Lecture: electronic structure of matter-wave functions and density functionals, Rev. Mod. Phys. 71 (5) (1999) 1253–1266.
[44] D.M. Ceperley, B.J. Alder, Ground state of the electron gas by a stochastic method, Phys. Rev. Lett. 45 (7) (1980) 566–569.
[45] J.P. Perdew, K. Burke, M. Ernzerhof, Generalized gradient approximation made simple, Phys. Rev. Lett. 77 (18) (1996) 3865–3868.
[46] L. Kleinman, D.M. Bylander, Efficacious form for model pseudopotentials, Phys. Rev. Lett. 48 (20) (1982) 1425–1428.
[47] D.R. Hamann, M. Schlüter, C. Chiang, Norm-conserving pseudopotentials, Phys. Rev. Lett. 43 (20) (1979) 1494–1497.
[48] R.J. Nicholls, A.J. Morris, C.J. Pickard, J.R. Yates, OptaDOS - a new tool for EELS calculations, J. Phys. Conf. 371 (2012), 012062.
[49] A.J. Morris, R.J. Nicholls, C.J. Pickard, J.R. Yates, OptaDOS: a tool for obtaining density of states, core-level and optical spectra from electronic structure codes, Comput. Phys. Commun. 185 (5) (2014) 1477–1485.
[50] J. Heyd, G.E. Scuseria, Assessment and validation of a screened Coulomb hybrid density functional, J. Chem. Phys. 120 (16) (2004) 7274–7280.
[51] J. Paier, M. Marsman, K. Hummer, G. Kresse, I.C. Gerber, J.G. Ángyán, Screened hybrid density functionals applied to solids, J. Chem. Phys. 124 (15) (2006) 154709.
[52] A.V. Krukau, O.A. Vydrov, A.F. Izmaylov, G.E. Scuseria, Influence of the exchange screening parameter on the performance of screened hybrid functionals, J. Chem. Phys. 125 (22) (2006) 224106.
[53] W. Jia, Z. Cao, L. Wang, J. Fu, X. Chi, W. Gao, L.-W. Wang, The analysis of a plane wave pseudopotential density functional theory code on a GPU machine, Comput. Phys. Commun. 184 (1) (2013) 9–18.
[54] W. Jia, J. Fu, Z. Cao, L. Wang, X. Chi, W. Gao, L.-W. Wang, Fast plane wave density functional theory molecular dynamics calculations on multi-GPU machines, J. Comput. Phys. 251 (2013) 102–115.
[55] W. Baur, The geometry of polyhedral distortions. Predictive relationships for the phosphate group, Acta Crystallogr. B Struct. Crystallogr. Cryst. Chem. 30 (5) (1974) 1195–1215.
[56] K. Momma, F. Izumi, VESTA3for three -dimensionalvisualization of crystal , volumetric and morphology data, J. Appl. Crystallogr. 44 (6) (2011) 1272–1276.
[57] H. Xiao, J. Tahir-Kheli, W.A. Goddard III, Accurate band gaps for semiconductors from density functional theory, J. Phys. Chem. Lett. 2 (3) (2011) 212–217.
[58] M. Chan, G. Ceder, Efficient band gap prediction for solids, Phys. Rev. Lett. 105 (19) (2010) 196403.
[59] A. Walsh, D.J. Payne, R.G. Egdell, G.W. Watson, Stereochemistry of post-transition metal oxides: revision of the classical lone pair model, Chem. Soc. Rev. 40 (9) (2011) 4455–4463.